ADVANCED FUNCTIONAL MATERIALS
www.afm-journal.de

Fluorescent Protein PEGylation for Stable Photon Manipulation in Deep-Red Light-Emitting Devices

*David Gutiérrez-Armayor, Sara Ferrara, Mattia Nieddu, Anna Zieleniewska, and Rubén D. Costa**

PEGylation is a classic strategy to reduce denaturation and immunogenicity in therapeutic proteins, bioimaging, and drug delivery. However, this concept has not been applied to incorporate biogenic materials as functional components in optoelectronics. Herein, PEGylation is rationalized as an effective tool to stabilize fluorescent proteins in solid-state photon manipulation down-converters integrated into bio-hybrid light-emitting diodes. In short, the archetypal red-emitting protein mCherry is nonspecifically PEGylated with methoxypolyethylene glycols (mPEG) chains of different lengths (mPEG-350/-750/-2000). These derivatives hold the same photoluminescence figures-of-merit of mCherry, but an improved resistance against organic solvents, pH, temperature, and polymers (in solution/dry-coatings) upon increasing the mPEG length. Indeed, the best-performing mCherry-mPEG-2000 adduct leads to deep-red devices with threefold enhanced color stability (>300 h) under harsh operation conditions (150 mW cm^{-2}) over the prior art. Different device architectures along with spectroscopic, thermocycling, and electrochemical impedance spectroscopy studies of the prepared coatings aid in rationalizing that PEGylation successfully reduces i) nonreversible thermal denaturation, ii) aggregation in solid-state, and iii) photo-induced oxidation and H$^+$-transfer deactivation of the chromophore, since oxygen diffusivity and H$^+$-reorganization across the protein skeleton are slowed down by strong H$^+$-bonding/hydrophobic mCherry-mPEG interactions. Hence, this simple supramolecular modification is of utmost relevance for future advances in protein-based optoelectronics.

1. Introduction

Synthetic biology is a key player in advancing new discoveries in the fields of medicine,[1] agriculture,[2] and environmental science,[3,4] among others. However, recent milestones in bio-electronics,[5,6] bio-optoelectronics (photovoltaic, lighting, sensing),[7–14] and bio-robotics[15–18] are pointing out that synthetic biology will be paramount in setting in highly adaptive, programmable, stable, and eco-friendly biocomponents for the sustainable technology transition. Nevertheless, adopting these technologies faces the scientific community with a number of challenges to overcome: i) mastering protein engineering tools to preserve functionality under relevant stress conditions (harsh temperature-/irradiation-/electrical-stimuli, processing techniques, and organic solvents);[19–21] ii) creating programmable and stimuli-responsive oligonucleotide-based assemblies (DNA, RNA and hybrids thereof), going from nano- to micro-scales, allowing spectral and/or spatial resolution readout (e.g., computing, data storage, and logic gates);[22–26] iii) designing simple and robust bio-interfaces that allow intimate and stable integration of all-human-made devices with biological tissues (e.g., healthcare, human-machine interfaces, therapeutics, and self-powering);[27] and iv) engineering living materials (i.e., combination of living cells and polymeric matrices), introducing a game-changing character in eco-efficient and low-cost material production, self-regeneration, environmental adaptation/responsivity, and genetically programmed functionalities and designs.[28–32]

In this context, although fluorescent proteins (FPs) are well-known in medical imaging and sensing,[33] only recently they have seen their successful debut in photon manipulation components for luminescent solar concentrators,[34–36] bio-hybrid light-emitting diodes (BioHLEDs),[37–42] and lasers,[43,44] as well as new photo-induced electron donors in solar cells.[45–47] Common to all these works are i) the high interest in FPs as alternative emitters/sensitizers due to their high photoluminescence quantum yields, wide gamut of colors, and easy/economical production,[48,49] and ii) the great efforts made to stabilize them upon processing and under relevant device operation conditions. In this context, our and other teams are exploring a variety of approaches: i) genetically encoded modifications,[41,45,50,51] ii) enhanced FP-polymer interfaces,[20,52] iii) sol–gel formation of

D. Gutiérrez-Armayor, S. Ferrara, M. Nieddu, A. Zieleniewska, R. D. Costa
Technical University of Munich
Campus Straubing for Biotechnology and Sustainability
Chair of Biogenic Functional Materials
Schulgasse 22, 94315 Straubing, Germany
E-mail: ruben.costa@tum.de

The ORCID identification number(s) for the author(s) of this article can be found under https://doi.org/10.1002/adfm.202412921

DOI: 10.1002/adfm.202412921

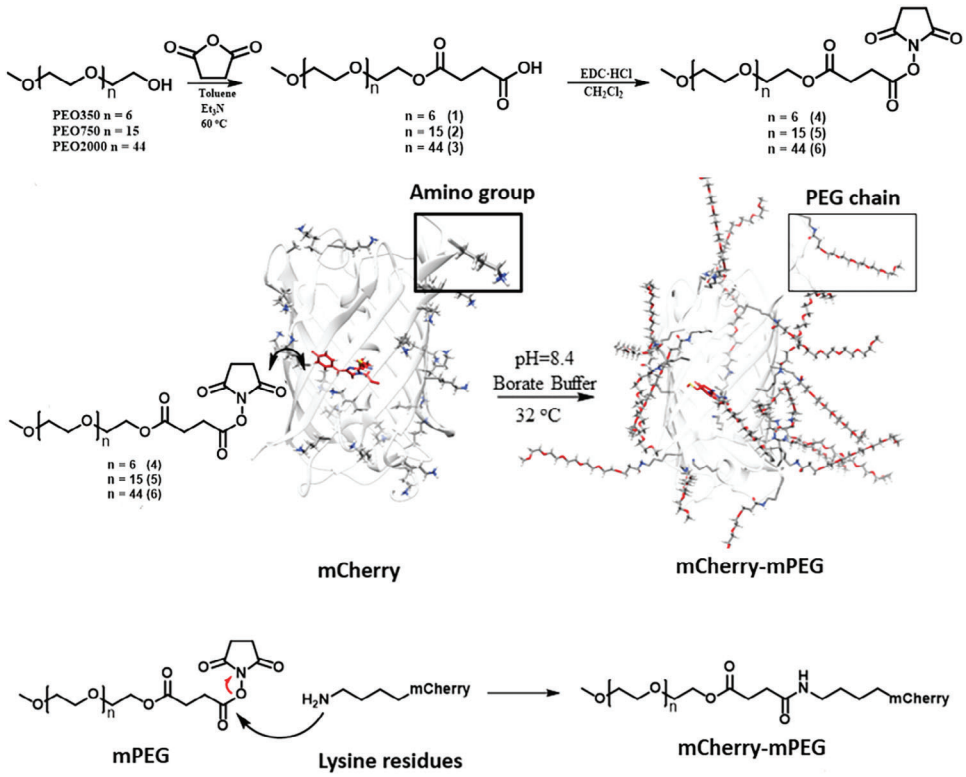

Figure 1. Synthetic strategy of mPEG functionalization (top) and PEGylation process of mCherry (bottom).

FP@metal oxide nanoparticles,[39,53–55] and iv) entrapment of FPs in metal–organic frameworks,[42,56,57] among others. This has led to impressive FP resilience toward foreign environments, such as year-long stable emission in organic solvents and dry coatings, thermal stabilities over 100 °C in solid-state, and irradiation stabilities over 6 months in devices operating under ambient conditions.

These achievements have been mostly realized with green-emitting FPs (i.e., eGFP, mGL), while the deactivation mechanism of red-emitting FPs (i.e., archetypal mCherry, smURFP) has been only recently deciphered in terms of oxygen- and H^+-mediated processes in polymer coatings.[40,58,59] This has allowed us to realize record BioHLED stabilities by embedding mCherry in a selected polyvinyl alcohol (PVA) matrix that significantly reduces water content and oxygen permeability upon vacuum drying.[40]

Building on this knowledge, we hypothesize that the PEGylation concept applied to mCherry could further boost the stability of protein-based lighting devices. On the one hand, methoxy-polyethylene glycols (mPEG) units exclude water from the protein surface by reinforcing mPEG-protein interactions via H-bonds and hydrophobic interactions,[60–64] reducing the likelihood of oxygen diffusion and photo-induced H^+-transfer deactivation of the chromophore, as well as preventing nonreversible temperature denaturation. On the other hand, long mPEG units allow a flexible long-range water molecule network to perfectly intermix with hydrophilic PVA units, without affecting its structural, thermal, mechanical, optical, and dielectric features when staying in low doping levels.[65–67]

To this end, this work describes the nonspecific PEGylation of mCherry with mPEGs of different chain lengths (i.e., **mCherry-mPEG350/-mPEG750/-mPEG2000**, **Figure 1**). These derivatives hold an improved resistance against organic solvents, pH, temperature, and polymers (solution/dry-coatings) upon increasing the mPEG chain length. Most importantly, emission and photoluminescence figures-of-merit, such as photoluminescence quantum yields (ϕ), excited state lifetimes (τ), and luminescence dissymmetry factor (g_{lum}), are also preserved. This encouraged us to prepare **mCherry-mPEG-2000-PVA** coatings leading to deep-red BioHLEDs with threefold higher color stabilities than those recently reported for mCherry-PVA references (i.e., 100 h vs 300 h at 150 mW cm^{-2}). This is attributed to the synergistic interplay of reduced chromophore oxidation and photo-induced H^+-transfer chromophore deactivation as well as enhanced renaturation kinetics as supported by spectroscopic, protein-modulated scanning fluorimetry, and electrochemical impedance spectroscopy studies of the mCherry-polymer coatings. Hence, this work highlights how simple supramolecular protein modification and coating engineering could be of utmost relevance for future advances in protein-based optoelectronics.

2. Results and Discussion

2.1. Synthesis and Characterization of mCherry-mPEG Derivatives

As shown in Figure 1, functionalized mPEG derivatives (**1-6**) have been synthesized and further used for the FP PEGylation

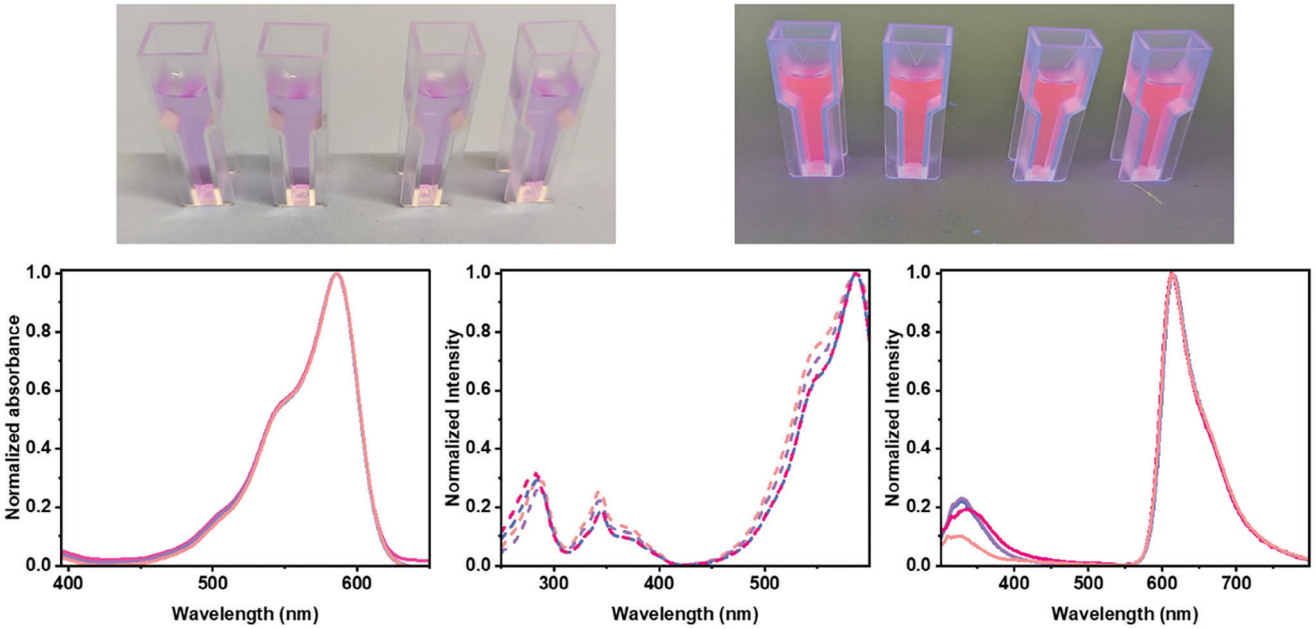

Figure 2. Top: From left to right, pictures of aqueous PBS buffer solution of mCherry and mCherry-mPEG350/750/2000 derivatives under ambient light (left) and UV irradiation (right). Bottom: Normalized absorption (left), excitation (center), and emission (right) spectra of native mCherry (orange), mCherry-mPEG350 (violet), mCherry-mPEG750 (blue), and mCherry-mPEG2000 (red) derivatives in aqueous PBS buffer solution.

process according to similar reported procedures (Experimental Section and Supporting Information).[68,69] In short, the synthetic pathway involves first the mPEG functionalization with a terminal carboxylic group in the presence of succinic anhydride and triethylamine at 60 °C for 24 h and their activation using coupling agents (EDC·HCl, NHS) at RT for 24 h. All mPEG derivatives were purified following common methodologies and were characterized using usual spectroscopic techniques (Experimental Section; Figures S1–S12, Supporting Information). Finally, mCherry PEGylation was successfully carried out using boric buffer (pH 8.4) at RT for 72 h by amidation reaction of the above-activated mPEGs (**4**-**6**) with accessible FP lysine residues, leading to the formation of mCherry-mPEG adducts (Figure 1). The successful functionalization of the native mCherry was confirmed by mass spectroscopy, indicating a chemical functionalization ranging from 15 to 12 units of the 20 accessible external lysine residues upon increasing mPEG length – Figure S13 (Supporting Information). This is expected as long chains introduce steric hindrances. Thus, mPEG-2000 was chosen as the longest chain for this study showing a good compromise between the highest level of functionalization and chain length.

As expected, the color of the solution of both mCherry and the mPEG- derivatives is similar to the naked eye (**Figure 2**). This is also confirmed by the similar shape of the absorption, excitation, and emission spectra in the solution (**Table 1** and Figure 2). In particular, the emission spectra (λ_{exc} = 280 nm) consist of two main emission bands centered at ≈330 and 610 nm that corresponds to the fluorescence of the aromatic amino acid resides and the ionic form of the mCherry chromophore, respectively. The intensity ratio between these emission bands is typically used to indicate the degree of distortion of the tertiary structure of the proteins upon denaturation.[52,70–72] In this case, PEGylation slightly increases the ratio from 0.1 to 0.2, suggesting a small distortion of the β-barrel structure upon functionalization as commonly noted in the literature.[73] Indeed, the photoluminescence figures-of-merit (τ, ϕ, and g_{lum}) values associated with the chromophore are in the same range as those of the native mCherry (reference), confirming that the chromophore cavity is not impacted by the

Table 1. Spectroscopical figures of merit of mCherry and mCherry-mPEG derivatives in aqueous PBS buffer.

	λ_{abs} [a] [nm]	ϵ [b] [a.u.]	g_{lum} [c]	λ_{exc} [d] [nm]	λ_{em} [e] [nm]	τ [f] [ns]	ϕ [g] [%]	Fr [h]
mCherry	586	1 ± 0.03	1.4×10^{-2}	585	613	1.57	21	51.16
mCherry-mPEG350	586	1.13 ± 0.05	1.5×10^{-2}	585	613	1.59	18	55.07
mCherry-mPEG750	586	0.99 ± 0.03	1.4×10^{-2}	585	611	1.61	20	56.30
mCherry-mPEG2000	586	0.97 ± 0.04	1.6×10^{-2}	585	613	1.64	18	57.34

[a] Maximum absorbance wavelength; [b] Extinction coefficient relative to the one of native protein; [c] Luminescence dissymmetry factor; [d] Maximum excitation wavelength at λ_{em} = 645 nm; [e] Maximum emission wavelength at λ_{exc} = 565 nm; [f] Excited state lifetime at λ_{exc} = 375 nm and $\lambda_{em} = \lambda_{max}$ nm; [g] Photoluminescence quantum yield at λ_{exc} = 590 nm; [h] Folding reversibility. Plots for the estimation of τ (Figure S15, Supporting Information), g_{lum} (Figure S16, Supporting Information), and F_r (Figure S17, Supporting Information) can be found.

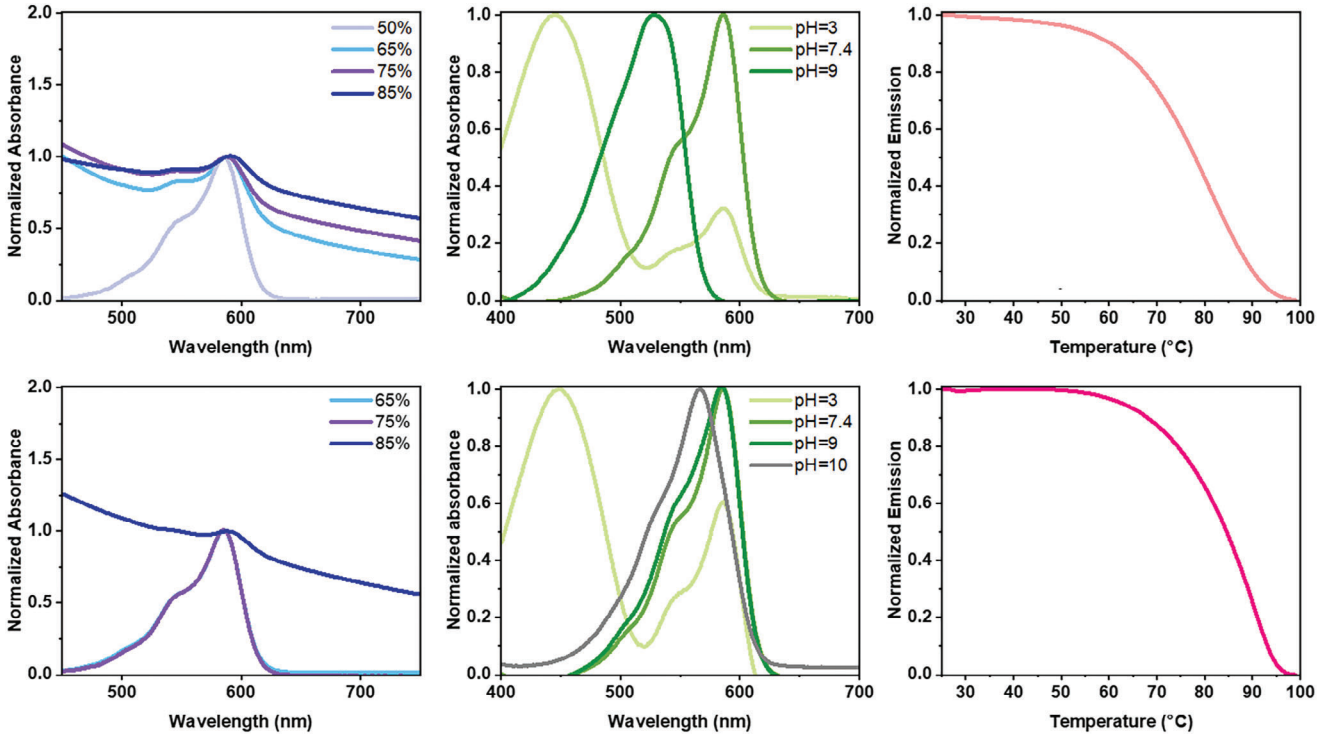

Figure 3. Left: Absorption spectra in AcN/water-based solutions of native mCherry (top) and mCherry-mPEG2000 (bottom) at different %v/v of ACN (see legend). Center: Absorption spectra of native mCherry (top) and mCherry-mPEG-2000 (bottom) in aqueous buffer solutions of different pH values (see legend). Right: Modulated scanning fluorimetry (MSF) experiments of native mCherry (top) and mCherry-mPEG2000 (bottom) in aqueous PBS buffer solution.

PEGylation process at the protein surface (Table 1). Most interestingly, spectroscopical characterization has shown that even after 1 year in cold storage (4 °C) the samples have suffered little to no degradation (Figure S14, Supporting Information).

The beneficial impact of the mPEG shell was confirmed upon monitoring i) the solubility and compatibility in organic solvents of mCherry and its derivatives, ii) the effect of the PEGylation on the pH-dependent chromophore denaturation, and iii) refoldability of mCherry and its derivatives after thermally induced denaturation in solution. At first, **Figure 3** and Figure S18 (Supporting Information) show that native mCherry undergoes a reduced solubility (i.e., formation of nonemissive aggregates) in acetonitrile (AcN)/water-based solutions at mixtures >65% *v/v* of AcN, while the modified mCherry-mPEG derivatives exhibit a lack of spectral changes up to mixtures > 85% *v/v* of AcN, pointing out the effective strengthening of the H^+-bonding network at the protein surface by the PEG chain interactions. Second, mCherry-mPEG derivatives show a higher tolerance toward harsh pH conditions than mCherry (Figure 3; Figures S19 and S20, Supporting Information). In short, the exposition of mCherry to pH > 9 leads to a significant blue shift of absorption and emission spectra caused by the deprotonation of the Lys70 and Glu215, amino acids close to the chromophore that interact with it through H-bonds.[74] In contrast, mCherry-mPEG derivatives demonstrate excellent resilience even after 24 h incubation (Figure S19, Supporting Information). Similar behavior is also noted at pH values >10, suggesting that the mPEG preserves the local pH in the surroundings of the protein scaffold.[64] Concerning the acidic conditions (pH 3), all the proteins exhibit a similar absorption spectrum with a new broadband located at 450 nm that is associated with the protonated form of the chromophore (Figure 3; Figures S20 and S21, Supporting Information).[75] This allows us to determine the degree of chromophore deactivation via the absorption intensity ratio of the neutral to anionic forms (I_{450}/I_{587}) that follows an empirical correlation with the mPEG length (Figure S21, Supporting Information). This finding underscores the remarkable ability of mPEG to endow mCherry with enhanced protection against H^+-transfer chromophore denaturation, which is highly remarkable if long mPEG chains are used. Finally, the temperature of nonreversibility (T_{nr}), depicts irreversible changes in protein structure by monitoring the changes in emission intensity after exposure to a specific temperature and subsequent cooling to room temperature.[76] As shown in Figure 3 and Table 1, mCherry modification results in an increase of the total area of T_{nr} (F_r: folding reversibility) upon increasing the mPEG length. This is attributed to the string interactions between mPEG chains that effectively shield the hydrophobic parts of the protein from the environment and prevent aggregation between protein units.[77]

2.2. Reference Elastomeric mCherry-mPEG Color Down-Converting Polymer Coatings Applied to BioHLEDs

At first, reference FP-based color down-converting coatings applied to BioHLEDs were prepared and characterized (Experimental Section and Supporting Information).[40,48] The coatings

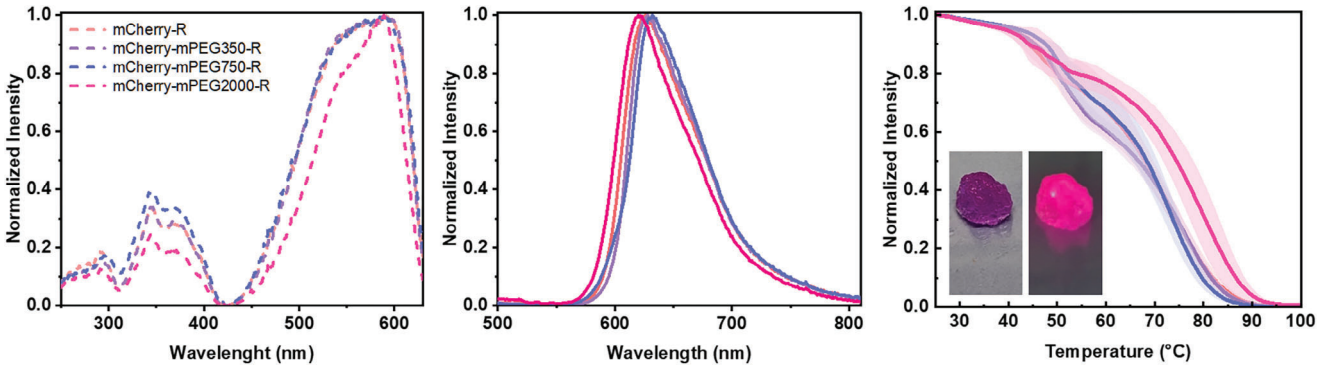

Figure 4. Normalized excitation spectra (left), emission spectra (center), and MSF curves (right) of native mCherry (orange), mCherry-mPEG350 (violet), mCherry-mPEG750 (blue), and mCherry-mPEG2000 (red) derivatives in reference TMPE:PEO coatings. *Inset:* Picture of the mCherry-mPEG2000 coatings under ambient light (left) and UV irradiation (right).

consist of a mixture of TMPE:PEO (trimethylpropane ethoxylate:polyethylene oxide) in a 4:1 mass ratio with the desired volume of the FP solution to meet the desired amount (typically of <1 wt% or 37.4 nmol). The mixture is stirred followed by a drying process at 3 mbar as described elsewhere (Experimental Section).[38] This results in an elastomeric coating with a 5 mm length and 2 mm height (**Figure 4**). We refer to **mCherry-R**, **mCherry-mPEG-350-R**, **mCherry-mPEG-750-R**, and **mCherry-mPEG-2000-R**.

All the coatings exhibit emission and excitation features that resemble those in solution (vide supra). In short, **mCherry-R** coatings feature an emission band centered at 626 nm that is slightly broadened and 13 nm redshifted when compared to that in solution (Figure 4 and **Tables** 1 and 2). In addition, the excitation spectra resemble that in solution (bands ascribed to the protein chromophore at 450–600 and 320–430 nm), showing a significant broadening with a poor vibrational resolution (Figures 2 and 4). As already noted in the literature, this is expected, since a certain degree of agglomeration upon coating preparation occurs, leading to structural distortions of the β-barrel and/or the H^+-chain distribution. This slightly changes i) the chromophore conformation,[75] ii) the protonation degree of its imidazolinone moiety in the ground state,[74,75] and/or iii) the H^+-bonding network interacting with the acylimine oxygen in the excited state.[78] However, the most relevant photoluminescence figures are not significantly affected with τ values of 1.45 ns and ϕ values of 20% (Tables 1 and 2; Figure S22, Supporting Information). Interestingly, it is expected that the PEGylation should reduce the agglomeration phenomena due to the compatibility with the polymer network. This is confirmed by i) the blueshifted maximum emission wavelength in **mCherry-mPEG2000-R** coatings compared to that of **mCherry-R** (Figure 4), ii) the overall slightly increased τ and ϕ values (Table 2), and iii) the well-defined excitation spectra noted for **mCherry-mPEG2000-R** coatings (Figure 4). Finally, the folding recovery capacity is also nicely enhanced with F_r values going from 40.11 (**mCherry-R**) to 45.05 (**mCherry-mPEG2000-R**) as shown in Figure 4 and Table 2. The MSF profile also indicates that there are two types of FP-species that resulted in two decays (45–55 °C) and a second decay starting from temperatures ≈70 °C. This should be related to the presence of poorly stabilized aggregates that are less present in the **mCherry-mPEG2000-R**. Here, the temperature decay shows a less steep slope and a larger temperature plateau. This nicely correlates with the spectroscopy findings (vide supra) as well as the device degradation profiles, as explained in the next section.

Table 2. Photoluminescence and thermal features of fresh mCherry and mCherry-mPEG TMPE:PEO (R) and PVA (P) coatings applied to BioHLEDs.

	λ_{exc} [a] [nm]	λ_{em} [b] [nm]	τ [c] [ns]	ϕ [d] [%]	Fr [e]
mCherry-R	565	626	1.45	20	40.11
mCherry-mPEG350-R	565	628	2.02	24	39.21
mCherry-mPEG750-R	565	632	2.01	23	40.16
mCherry-mPEG2000-R	565	620	2.02	22	45.05
mCherry-P	590	630	1.35	16	32.64
mCherry-mPEG2000-P	585	630	1.35	18	50.07

[a] Maximum excitation wavelength at λ_{em} = 645 nm; [b] Maximum emission wavelength at λ_{exc} = 565 nm; [c] Excited state lifetime with λ_{ex} = 375 nm and $\lambda_{em} = \lambda_{max}$ nm; [d] Photoluminescence quantum yield at λ_{exc} = 590 nm; [e] Folding reversibility. Plots for the estimation of τ (Figures S22 and S25, Supporting Information) can be found.

Encouraged by these results, deep-red BioHLEDs were prepared by covering a commercial 590 nm LED pumping chip with the above coatings (see Experimental Section; Supporting Information). Following the literature, the device were driven at 200 mA (i.e., 55 mW cm^{-2} incident photon flux) under ambient conditions (i.e., 25 °C and 45% moisture), monitoring both temperature and emission intensity profiles of the mCherry-based coatings over time. The temperature slightly increases up to 30 °C and holds constant over time, indicating that the deactivation of the chromophore is only related to photo-induced processes, such as oxidation and H^+−transfer. The devices showed an emission spectrum featuring a total down-conversion, showing only a peak at 630 nm (down-conversion band related to the mCherry emission). In line with the literature, the emission intensity decay profile of the down-conversion band consists of three regimes (**Figure 5**). The first step is characterized by an exponential intensity loss of ≈20% attributed to the degradation of poorly stabilized aggregate-like FPs with the exception of devices with **mCherry-mPEG2000-R** that feature a ≈10% intensity loss

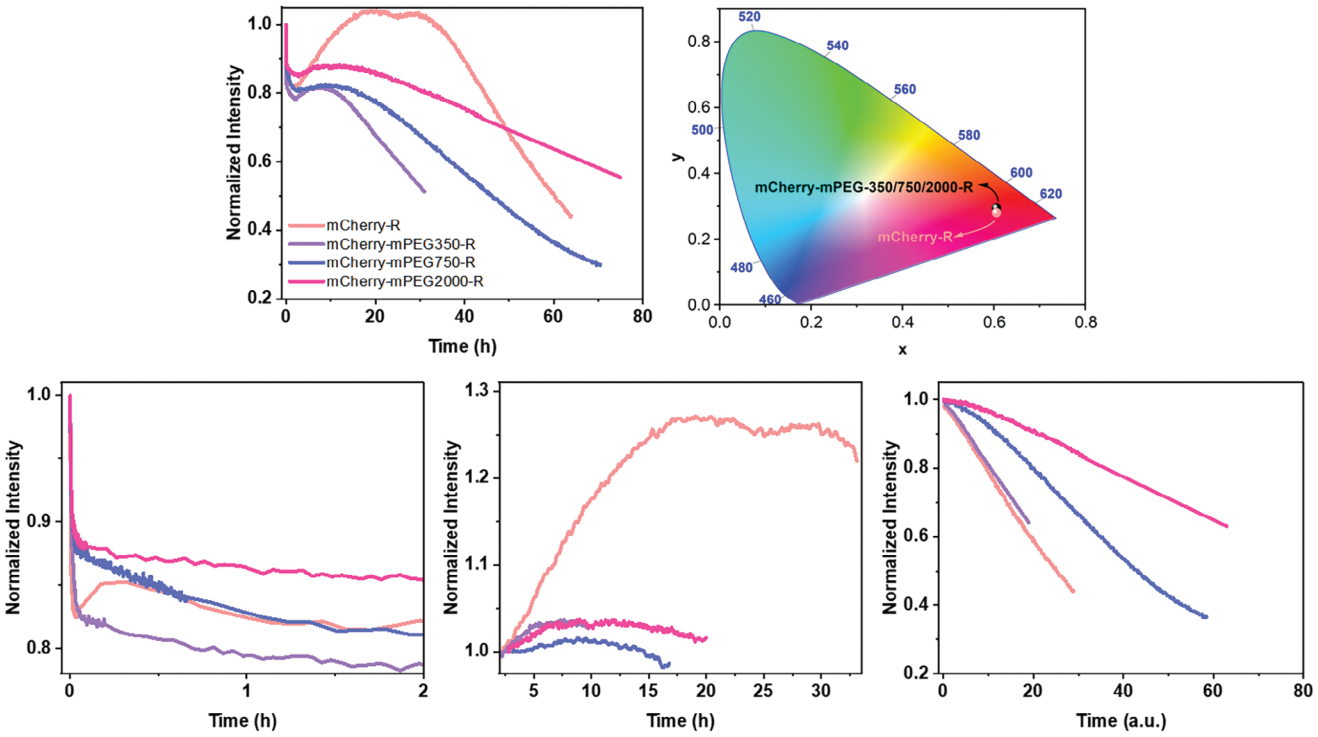

Figure 5. Top: Overall intensity decay profiles of devices with native mCherry-R (orange), mCherry-mPEG350-R (violet), mCherry-mPEG750-R (blue), and mCherry-mPEG2000-R (red) coatings upon 590 nm irradiation at 55 mW cm^{-2} in ambient (left) and device chromaticity changes in the x/y CIE 1931 color coordinates (right). Bottom: Normalized emission decay profile of the first (left), second (right), and third (right) regimes.

caused by the less degree of agglomeration as pointed out by spectroscopy and thermal data (vide supra). The second regime consists of the recovery of the emission intensity caused by a further oxygen-mediated maturation of the TagBFP-like chromophore to its red-emitting form.[79,80] This recovery is ≈20% for devices with **mCherry-R** (i.e., full recovery of the initial intensity; Figure 5) and takes ≈40 h to be completed. In stark contrast, the PEGylation process shines as the expected effective oxygen barrier, leading to a significant decrease of the recovery percentage with the mPEG chain length going down to <5% recovery (Figure 5), and can be completely eliminated if performing the measurement in completely inert conditions (Figure S23, Supporting Information). The third last regime exhibits a linear emission intensity decay related to chromophore isomerization induced by the deprotonation of the Glu215 as an H^+-exchange mechanism at the protein surface.[40] Here, the PEGylation process is also effective in reducing the H^+-transfer mechanism as the mPEG chains strongly interact with the protein surface via H^+-bonding and hydrophilic interactions. This is reflected by the decrease of the linear slope going from −0.0183 to −0.0133, to −0.0096, and to −0.0052 upon increasing the mPEG chain length (i.e., **mCherry-R**, **mCherry-mPEG350-R**, **mCherry-mPEG750-R**, and **mCherry-mPEG2000-R**, respectively).

Overall, **mCherry-mPEG2000-R** coatings showed the highest device stability (i.e., time to reach half of the initial emission intensity), reaching an almost twofold enhancement compared to reference with **mCherry-R** coatings (i.e., 95 h vs 56 h). This again highlights the beneficial impact of the PEGylation concept in protein-based lighting.

2.3. Best Performing mCherry-mPEG Color Down-Converting PVA Coatings Applied to BioHLEDs

We have recently identified that PVA polymer coatings with low permeability to oxygen and reduced H^+−motion improve device stability.[40] Thus, our next step was to evaluate the synergistic effect of combining the above best-performing **mCherry-mPEG-2000** and PVA-based matrices to outperform current deep-red mCherry-based BioHLEDs.

To this end, reference **mCherry-P**, and **mCherry-mPEG-2000-P** coatings were prepared following the previous report (Experimental Section; Supporting Information).[40] In short, **mCherry-mPEG-2000** or native **mCherry** PBS solutions (<0.5 wt%, 37.4 nmol) were added to a Mowiol 28–99 gel in milli-Q water under gentle stirring conditions at room temperature. This was followed by a drying process under vacuum in a dome-like mold, resulting in a rigid coating with 5 mm diameter and 5 mm height.

The emission and excitation spectra of all PVA-based coatings mainly consist of a broad and intense emission band centered at 630 nm and three broad excitation bands located at 590, 390, and 280 nm (Figure S24, Supporting Information). This is associated with τ and ϕ values of ≈1.4 ns and 20%, respectively (Table 2). As expected from the above notes about reference coatings, the **mCherry-mPEG-2000-P** coatings showed slightly enhanced photoluminescence features and a structurally shaped spectrum, pointing out a lower degree of agglomeration. Indeed, MSF studies showed the above-described two-step thermal denaturation steps for **mCherry-P** with a much less pronounced

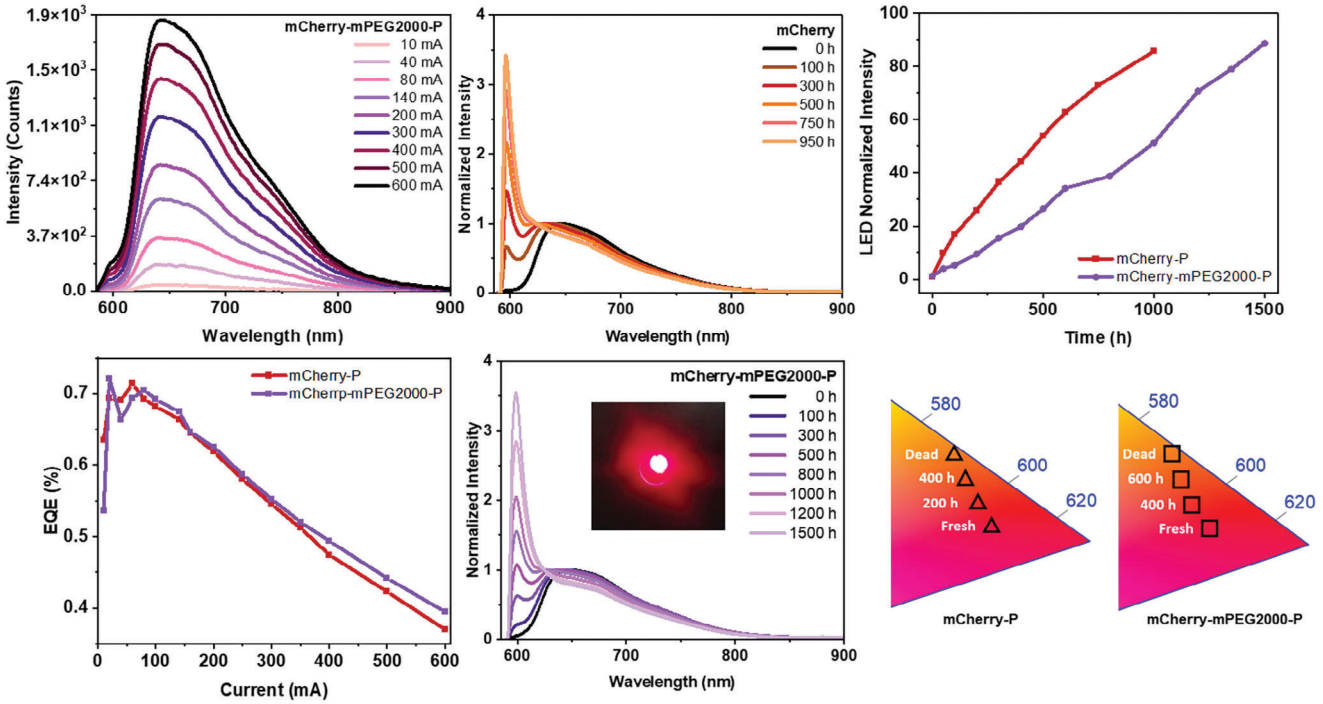

Figure 6. Left: Emission spectra (top) and the external quantum efficiency (bottom) of devices with **mCherry-mPEG2000-P** at applied currents of 10–600 mA (λ = 590 nm). Center: Changes of the emission spectra over time of devices with **mCherry-P** (top) and **mCherry-mPEG-2000-P** (bottom) devices at an applied current of 600 mA (see legend, λ = 590 nm, 150 mW cm^{-2}). Inset: Picture of a working device). Right: Changes of the LED emission intensity (top) and x/y CIE color coordinates evolution (bottom) of devices with **mCherry-P** (triangles) and **mCherry-mPEG-2000-P** (squares) devices at an applied current of 600 mA (λ = 590 nm, 150 mW cm^{-2}).

first regime and a final F_r of 32.64, while **mCherry-mPEG-2000-P** is featured by a faint first regime and a significantly enhanced F_r reaching values 50.07 (Figure S24, Supporting Information; Table 2). Hence, both, the spectroscopic and thermal features of **mCherry-mPEG-2000-P** seem to promise an enhanced device performance compared to reference devices.

To confirm this statement, deep-red BioHLEDs were fabricated as above mentioned with both PVA coatings and measured at different currents under the same ambient conditions (Experimental Section; Supporting Information). All the devices showed a full conversion of the LED emission at the applied current range of 10–600 mA (**Figure 6**). The device chromaticity corresponds to the deep-red region associated with a broad emission band centered at 620 nm and x/y CIE color coordinates of 0.61/0.28 and maximum external quantum efficiency (EQE) values of ≈0.7% (Figure 6). The device stability was carried out with a high-power excitation flux (600 mA, 150 mW cm^{-2}) under ambient conditions to speed up data acquisition. Despite the harsher driving conditions compared to the reference devices (threefold higher photon flux excitation), the temperature of the coatings holds constant (<30 °C), but the emission of pumping LED becomes broader hampering the clean monitoring of the emission intensity changes of the down-converting emission band. Thus, the device stability is discussed in terms of chromaticity corruption as the LED emission band at 590 nm is becoming more prominent. In detail, the emission band at 590 nm evolves quicker for devices with **mCherry-P** coatings than those with **mCherry-mPEG2000-P** coatings as indicated by the slopes of the emission intensity increase versus time shown in Figure 6 (i.e., 0.085 vs 0.058). Indeed, the time needed to reach a 1:1 emission intensity ratio between the bands centered at 590 and 620 nm is ≈200 and ≈500 h for devices with **mCherry-P** and **mChery-mPEG2000-P** coatings (Figure 6). Finally, the enhanced device stability is also corroborated by the color corruption of the devices, in which the x/y CIE color coordinates of the device with **mCherry-mPEG2000-P** did not change for over 200 h, reaching meaningful chromaticity changes after >300 h (Figure 6). In stark contrast, devices with **mCherry-P** show an evident color corruption after 100 h, quickly evolving to the x/y CIE coordinate 0.57/0.43 of the pumping chip.

Similar to the above reference coatings, the overall device stability is also enhanced approximately threefold upon PEGylation (**mCherry-mPEG2000**). However, oxygen-mediated reactions and temperature denaturation cannot be considered in PVA coatings. The changes in photostability point out a slower deprotonation process of the Glu215 that induces the formation of the neutral chromophore species that can easily lose coplanarity.[74,81] In order to further corroborate this H^+-transfer deactivation process, electrochemical impedance spectroscopy was applied to **mCherry-P** and **mCherry-mPEG2000-P** films as well as blended PVA mPEG2000 (**mPEG2000-P**) films for reference purposes (Experimental Section; Supporting Information for more details).

The Nyquist and equivalent circuits used for the fittings are shown in **Figures 7** and S26 (Supporting Information), while the resistances (R) are gathered in Figure 7. In line with the prior art, the Nyquist plot of the **mPEG2000-P** films consists of

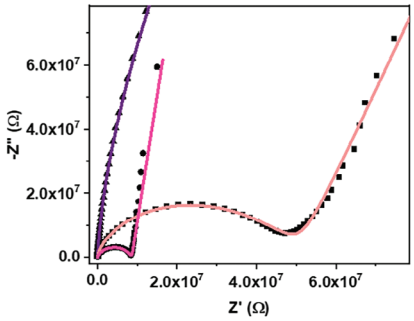

Sample	R_{Prot}	R_{PVA}	R_e
mPEG-2000-P	-	1.45 MΩ	3.08 GΩ
mCherry-P	152 kΩ	52.4 MΩ	1.1 TΩ
mCherry-mPEG-2000-P	673 kΩ	8.02 MΩ	1.1 TΩ

Figure 7. Nyquist (left) and table gathering the main resistance values of **mPEG2000-P** (purple), **mCherry-P** (orange), and **mCherry-mPEG-2000-P** (red) over the frequency range of 0.01 Hz–150 kHz. The solid lines represent the fitting of the impedance based on the model equivalent circuit shown in Figure S26 (Supporting Information).

two semicircles related to the charge transfer event at the electrode/PVA interface (R_e = 3.08 GΩ) and a H^+-transfer event at the **mPEG2000-PVA** interface (R_{PVA} = 1.45 MΩ).[67,82] In the case of **mCherry-P** films, three semicircles are noted, showing similar resistances for the electrode/PVA interface and an H^+-transfer event at the **mCherry-PVA** interface (R_{PVA} = 52.4 MΩ), and finally the H^+-chain re-orientation at the mCherry surface with R_{Prot} = 152 kΩ.[83] Finally, **mCherry-mPEG2000-P** films showed similar R_e to the other samples and a similar R_{PVA} to those of **mPEG2000-PVA** films (Figure 7). In contrast, the most significant change is the R_{Prot} of **mCherry-mPEG2000-P** which is fourfold higher compared to that of **mCherry-P** (Figure 7), indicating that the dynamics of H^+-chain re-orientation at the mPEG200-mCherry interface is slow down. This is attributed to the exclusion of water molecules at the mCherry surface by the mPEG units,[60–63] generating a negative H^+-gradient at the mCherry and PVA interface that reduces the H^+ transfer. Hence, PEGylation effectively assists in decreasing photo-induced H^+-transfer deactivation processes in polymer coatings, becoming a relevant tool to further enhance protein-based optoelectronics.

3. Conclusion

This work sets in PEGylation as a successful strategy to further stabilize fluorescent proteins in solid-state photon manipulating filters for BioHLEDs. This is attributed to strong protein-mPEG interactions (H^+-bonding and hydrophobic) that effectively shield the protein chromophore from oxidation and photo-induced H^+-transfer chromophore deactivation. In addition, this simple protein surface functionalization reduces the agglomeration upon preparation of polymer coatings, while the protein refolding capability in the polymer coatings is significantly enhanced (>50% increase in PVA coatings). These benefits in solid-state complement other classical ones noted in solution, such as enhanced tolerance to organic solvents and pH, while retaining its photoluminescence figures-of-merit. Hence, we could safely state that PEGylation holds great potential to further advance protein-based optoelectronics, in general, and FP-based lighting, in particular. This is supported by a threefold enhanced color stability when compared to the best-reported mCherry-PVA-based devices up to date in deep-red BioHLEDs, through the combination of mCherry-mPEG-2000 and PVA matrix. What is more, selective PEGylation as well as other linear and branched motifs could lead to further stabilization in different FPs. This represents an on-going work in our laboratory.

4. Experimental Section

FP Production: mCherry was produced in *Escherichia coli* BL21(DE3). The cultures were induced with Isopropyl-β-D-1-thiogalactopyranoside (IPTG) at OD_{600} = 0.4. Cells were harvested, yielding a red pellet, and disrupted via sonication (Amplitude 80, pulse on-time: 1 s, off-time 3 s). After centrifugation, the supernatant yielding the protein was purified using a HisTrap HP 5 mL column of Äkta pure cytiva and desalted using a HiPrepTM 26/10 Desalting column (Äkta pure cytiva). After desalting, the proteins were flash-frozen in PBS buffer with a 10 mg mL^{-1} concentration and stored at −80 °C. Before use, the proteins were thawed and centrifuged to remove aggregated proteins. The mCherry protein sequence is MVSKGEEDNM AIIKEFMRFK VHMEGSVNGH EFEIEGEGEG RPYEGTQTAK LKVTKGGPLP FAWDILSPQF MYGSKAYVKH PADIPDYLKL SFPEGFKWER VMNFEDGGVV TVTQDSSLQD GEFIYKVKLR GTNFPSDGPV MQKKTMGWEA SSERMYPEDG ALKGEIKQRL KLKDGGHYDA EVKTTYKAKK PVQLPGAYNV NIKLDITSHN EDYTIVEQYE RAEGRHSTGG MDELYK.

FP-PEGylation Procedure and Characterization in Solution: Starting material such as N-hydroxysuccinimide (NHS), boric acid, methyl-polyethylene glycol (mPEG-350, mPEG-750, mPEG-2000), 1-Ethyl-3-(3-dimethylaminopropyl) carbodiimide hydrochloride (EDC·HCl), Trimethylolpropane ethoxylate (TMPE-450) were purchased from Sigma. Millipore Amicon Ultra-50 filters (MWCO = 30 000) were purchased from Merck. ^1H and ^{13}C spectra were recorded at 25 °C on a JNM ECS 400 MHz NMR spectrometer (Jeol, Freising, Germany). Samples were prepared by dissolving a small amount of the product in deuterated chloroform inside a 5 mm glass tube. Chemical shifts in ^1H NMR and ^{13}C NMR spectra are reported in SI. 1 mL of 10 mg mL^{-1} mCherry was prepared for the functionalization through buffer exchange to 1 M borate buffer using Millipore Amicon Ultra-50 filters (MWCO = 30 000). The resultant solution, of an approximate volume of 2 mL, is then mixed with 100 µmol of the previously prepared polymer. The mixture is heated up to 32 °C and covered with aluminum foil to prevent photodegradation. The solution is vigorously stirred for 72 h, before separating the unreacted polymer by exchanging the buffer for 10 mM PBS buffer through ultrafiltration using Millipore Amicon Ultra-50 filters. Absorption spectra were acquired with a UV–vis spectrometer UV-2600 (Shimadzu), using a wavelength range of 300–800 nm, scan speed medium, threshold 0.01, and a slit width of 2.0. High-resolution Matrix-Assisted Laser Desorption/Ionization (MALDI) spectra were recorded on a Maldi-TOF Microflex mass spectrometer. The photophysical characterization (excitation and emission spectra, ϕ, τ) of all the samples was carried out with an FS5 Spectrofluorometer from Edinburgh Instruments, using an SC-5 module for liquid samples and an SC-30 Integrating Sphere to determine ϕ (λ_{exc} = 590 nm). All measurements were performed at RT in ambient.

pH and Organic Solvents Solubility Study: The studies were carried out in a 2 mL polystyrene cuvette, mixing the protein with PBS buffers and solutions of organic solvents with the required characteristics. Immediately upon mixing, the absorbance was recorded as indicated previously. The lower tail of the data was removed due to the absorbance of the plastic cuvette. In all studies, the concentration of protein was 0.1 mg mL^{-1}.

Extinction Coefficient Determination: Following the procedure described by W.Ward,[84] measurements were carried out in a 2 mL polystyrene cuvette, mixing the protein with PBS pH 7.4 to a final concentration of 0.1 mg mL^{-1}. The same amount of protein was then mixed with a solution of NaOH 0.5 M, ensuring total protonation of the chromophore without denaturation. From the values of the absorbance of the neutral peak and the original one of the protein, the extinction coefficient is determined as:

$$\varepsilon = \frac{Abs_{\text{native}}}{Abs_{\text{in basic media}}} \times 44000 \quad (1)$$

All measurements were carried out in triplicates to obtain statistically meaningful values.

Thermocycler-Based Modulated Scanning Fluorimetry: Modulated Scanning Fluorimetry (MSF) was performed as described in Svilenov et al. 2020.[76] The Thermocycler CFX96 Touch Real_time PCR System (Bio-Rad) was employed to perform MSF measurements. One standard program composed of heating and cooling cycles ranging from 25 to 99 °C was used to measure the progressive loss of fluorescence and the irreversible unfolding of the FPs studied in this work. The samples were heated at 5 °C s^{-1} and held for 1 min at the temperature peak, followed by a recovery period of 5 min at 25 °C. Due to the high sensitivity of the Thermocycler detector and high QY of the FPs used in this study, only 1 µM of FPs, either in a 50 µL volume of solution or in 10 mg of coating, were added per well to avoid saturation. The thermograms were buffer-subtracted and normalized by the highest fluorescence readout of each sample. Data analysis was performed using Origin 2019 (OriginLab Corporation, Northampton, MA, USA). Mean values and standard deviations of quintuplicate were calculated and plotted. Melting curves were obtained by plotting the fluorescence values obtained at peak temperatures, while nonreversibility curves were obtained by plotting the fluorescence values obtained at 25 °C.

CPL Measurements: The data were recorded using an Olis CPL Solo (circular polarized luminescence) spectrometer and the software OlisGlobalWorks. Raw data were processed by an in-house Python script that averaged and processed the data with a Savitzky–Golay filtering of the repeated measurements. The final CPL raw curves were fitted by the least-squares method using the LMFIT and SciPy Python toolboxes to the best double Gaussian. Protein concentration was kept at 0.2 mg mL^{-1} for all measurements.

Preparation and Characterization of FP-Polymer Coatings: The rubber-like coatings **mCherry-mPEG-350/PEO-750/PEO-2000-R** and the reference **mCherry-R** were prepared with a mass ratio of 4:1 (TMPE:PEO). A PBS solution containing 37.4 nmol of either mCherry-mPEG350/750/2000 (see the preparation of modified mCherry with mPEGs) or native mCherry in analog amount was added to TMPE and stirred together with PEO. The samples were dried overnight in a vacuum chamber at 3 mbar, following reported procedures.[85] The PVA-based bio-phosphors **mCherry-mPEG-2000-P** and the reference **mCherry-P** PVA-based samples were prepared by adding a PBS solution bearing 37.4 nmol of either mCherry-mPEG350/750/2000 or analog amount of native mCherry to a solution of Mowiol 28–99. The samples were dried overnight in a vacuum chamber at 1 mbar. mCherry-mPEG-2000-P and mCherry-P samples for EIS essays have been prepared following the described procedure to form the mCherry–Mowiol solutions. Such mixtures are then poured into a Teflon mold and dried overnight in ambient. The photophysical characterization (excitation and emission spectra, ϕ, τ) of all the samples was carried out with an FS5 Spectrofluorometer from Edinburgh Instruments, using an SC-10 module for solid samples and SC-30 Integrating Sphere to determine ϕ (λ_{exc} = 590 nm). All measurements were performed at RT in ambient. The impedance measurements were carried out using a potentiostat PGSTAT204, Metrohm Autolab with FRA32M module for impedance analysis. The protein-PVA films were placed between two FTO electrodes. A frequency range of 0.01 Hz–150 kHz was used with an applied ac bias of 100 mV (no dc bias was applied). All the reagents were acquired from Sigma Aldrich.

Device Fabrication and Characterization: The devices were fabricated using commercial 590 nm LED chips (WINGER WEPYE1-S1 Power LED Star) as a pumping source and the FP-polymer coatings were placed onto the LED without further modification. The devices were driven either at different currents to study conversion and efficiency or at 200/600 mA (55 mW cm^{-2}/150 mW cm^{-2}) for long-term stability at ambient conditions. The emission spectra were recorded through Avantes Spectrometer 2048L (300 VA grating, 200 µm slit, CCD detector) coupled with an AvaSphere 30-Irrad Integrated sphere, monitoring the temperature using a thermographic camera FLIR ETS320. The employed power source was a Keithley 2231-A-30-3.

Supporting Information

Supporting Information is available from the Wiley Online Library or from the author.

Acknowledgements

D.G.A. and S.F. contributed equally to this work. R.D.C. and S.F. acknowledge the European Union's Horizon 2020 research and innovation FET-OPEN under grant agreement ARTIBLED No. 863170. R.D.C. and D.G.A. acknowledge the ERC-Co InOutBioLight No. 816856. A.Z. acknowledges the European Union's Horizon 2020 research and innovation MSCA Fellowship program under the grant agreement HeatBLED No. 101066817.

Open access funding enabled and organized by Projekt DEAL.

Conflict of Interest

The authors declare no conflict of interest.

Data Availability Statement

The data that support the findings of this study are available from the corresponding author upon reasonable request.

Keywords

deep-red lighting sources, fluorescent proteins, PEGylation, photon manipulation, solid-state protein stabilization

Received: July 19, 2024
Revised: September 16, 2024
Published online: October 14, 2024

[1] B. Leader, Q. J. Baca, D. E. Golan, *Nat. Rev. Drug Discovery* **2008**, *7*, 21.
[2] M. Hayes, in *Novel Proteins for Food, Pharmaceuticals, and Agriculture: Sources, Applications, and Advances*, 1st ed, Wiley-Blackwell, Hoboken, NJ, USA **2018**.
[3] N. Deligonul, I. Yildiz, S. Bilgin, I. Gokce, O. Isildak, *Microchem. J.* **2023**, *190*, 108710.
[4] I. Bodlund, A. R. Pavankumar, R. Chelliah, S. Kasi, K. Sankaran, G. K. Rajarao, *Int. J. Environ. Sci. Technol.* **2014**, *11*, 873.

[5] G. Malliaras, I. McCulloch, *Chem. Rev.* **2022**, *122*, 4323.
[6] Y. Zhang, Z. Wang, Y.-C. Chen, *Prog. Quantum Electron.* **2021**, *80*, 100361.
[7] I. M. Goodchild-Michelman, G. M. Church, M. G. Schubert, T.-C. Tang, *Mater. Today Bio* **2023**, *19*, 100583.
[8] X. Chen, J. M. Lawrence, L. T. Wey, L. Schertel, Q. Jing, S. Vignolini, C. J. Howe, S. Kar-Narayan, J. Z. Zhang, *Nat. Mater.* **2022**, *21*, 811.
[9] N. Schuergers, C. Werlang, C. M. Ajo-Franklin, A. A. Boghossian, *Energy Environ. Sci.* **2017**, *10*, 1102.
[10] L. M. Cavinato, E. Fresta, S. Ferrara, R. D. Costa, *Adv. Energy Mater.* **2021**, *11*, 2100520.
[11] M. Humar, S. H. Yun, *Optica* **2017**, *4*, 222.
[12] V. A. de la Peña O'Shea, R. D. Costa, *Adv. Energy Mater.* **2021**, *11*, 2102874.
[13] E. Fresta, V. Fernández-Luna, P. B. Coto, R. D. Costa, E. Fresta, V. Fernández-Luna, R. D. Costa, P. B. Coto, *Adv. Funct. Mater.* **2018**, *28*, 1707011.
[14] N. Toropov, F. Vollmer, *Light Sci. Appl.* **2021**, *10*, 77.
[15] Z. Lin, T. Jiang, J. Shang, *Bio-Des. Manuf.* **2022**, *5*, 107.
[16] Z. Wang, A. Klingner, V. Magdanz, S. Misra, I. S. M. Khalil, *Adv. Intell. Syst.* **2024**, *6*, 2300093.
[17] W. Haouas, M. Gauthier, K. Rabenorosoa, *Curr. Robot. Rep.* **2024**, *5*, 15.
[18] N. Jiang, C. Chen, J. He, J. Meng, L. Pan, S. Su, X. Zhu, *Natl. Sci. Rev.* **2023**, *10*, nwad048.
[19] E. M. Pelegri-O'Day, H. D. Maynard, *Acc. Chem. Res.* **2016**, *49*, 1777.
[20] B. Panganiban, B. Qiao, T. Jiang, C. DelRe, M. M. Obadia, T. D. Nguyen, A. A. A. Smith, A. Hall, I. Sit, M. G. Crosby, P. B. Dennis, E. Drockenmuller, M. Olvera de la Cruz, T. Xu, *Science* **2018**, *359*, 1239.
[21] U. Rinas, E. Garcia-Fruitós, J. L. Corchero, E. Vázquez, J. Seras-Franzoso, A. Villaverde, *Trends Biochem. Sci.* **2017**, *42*, 726.
[22] S. Dey, C. Fan, K. V. Gothelf, J. Li, C. Lin, L. Liu, N. Liu, M. A. D. Nijenhuis, B. Saccà, F. C. Simmel, H. Yan, P. Zhan, *Nat. Rev. Methods Primer* **2021**, *1*, 13.
[23] P. Zhan, A. Peil, Q. Jiang, D. Wang, S. Mousavi, Q. Xiong, Q. Shen, Y. Shang, B. Ding, C. Lin, Y. Ke, N. Liu, *Chem. Rev.* **2023**, *123*, 3976.
[24] H. Lv, N. Xie, M. Li, M. Dong, C. Sun, Q. Zhang, L. Zhao, J. Li, X. Zuo, H. Chen, F. Wang, C. Fan, *Nature* **2023**, *622*, 292.
[25] D. Fan, J. Wang, E. Wang, S. Dong, *Adv. Sci.* **2020**, *7*, 2001766.
[26] S. Yang, B. W. A. Bögels, F. Wang, C. Xu, H. Dou, S. Mann, C. Fan, T. F. A. de Greef, *Nat. Rev. Chem.* **2024**, *8*, 179.
[27] B. S. Gomes, B. Simões, P. M. Mendes, *Nat. Rev. Chem.* **2018**, *2*, 0120.
[28] S. Molinari, R. F. Tesoriero, D. Li, S. Sridhar, R. Cai, J. Soman, K. R. Ryan, P. D. Ashby, C. M. Ajo-Franklin, *Nat. Commun.* **2022**, *13*, 5544.
[29] A. Rodrigo-Navarro, S. Sankaran, M. J. Dalby, A. del Campo, M. Salmeron-Sanchez, *Nat. Rev. Mater.* **2021**, *6*, 1175.
[30] K. S. Wun, I. Y. Hwang, M. W. Chang, *Nat. Mater.* **2022**, *21*, 382.
[31] R. M. McBee, M. Lucht, N. Mukhitov, M. Richardson, T. Srinivasan, D. Meng, H. Chen, A. Kaufman, M. Reitman, C. Munck, D. Schaak, C. Voigt, H. H. Wang, *Nat. Mater.* **2022**, *21*, 471.
[32] A. P. Liu, E. A. Appel, P. D. Ashby, B. M. Baker, E. Franco, L. Gu, K. Haynes, N. S. Joshi, A. M. Kloxin, P. H. J. Kouwer, J. Mittal, L. Morsut, V. Noireaux, S. Parekh, R. Schulman, S. K. Y. Tang, M. T. Valentine, S. L. Vega, W. Weber, N. Stephanopoulos, O. Chaudhuri, *Nat. Mater.* **2022**, *21*, 390.
[33] Y. Yang, K. Xiang, Y. X. Yang, Y. W. Wang, X. Zhang, Y. Cui, H. Wang, Q. Q. Zhu, L. Fan, Y. Liu, A. Cao, *Nanoscale* **2013**, *5*, 10345.
[34] S. Sadeghi, R. Melikov, H. Bahmani Jalali, O. Karatum, S. B. Srivastava, D. Conkar, E. N. Firat-Karalar, S. Nizamoglu, *ACS Appl. Mater. Interfaces* **2019**, *11*, 8710.
[35] A. R. Frias, S. F. H. Correia, M. Martins, S. P. M. Ventura, E. Pecoraro, S. J. L. Ribeiro, P. S. André, R. A. S. Ferreira, J. A. P. Coutinho, L. D. Carlos, *Adv. Sustain. Syst.* **2019**, *3*, 1800134.
[36] C. P. A. Carlos, S. F. H. Correia, M. Martins, O. A. Savchuk, J. A. P. Coutinho, P. S. André, J. B. Nieder, S. P. M. Ventura, R. A. S. Ferreira, *Green Chem.* **2020**, *22*, 4943.
[37] S. Nizamoglu, *SDÜ Fen Bilim. Enstitüsü Derg.* **2016**, *20*, 490.
[38] M. D. Weber, L. Niklaus, M. Pröschel, P. B. Coto, U. Sonnewald, R. D. Costa, *Adv. Mater.* **2015**, *27*, 5493.
[39] M. Nieddu, M. Patrian, S. Ferrara, J. P. Fuenzalida Werner, F. Kohler, E. Anaya-Plaza, M. A. Kostiainen, H. Dietz, J. R. Berenguer, R. D. Costa, *Adv. Sci.* **2023**, *10*, 2300069.
[40] S. Ferrara, J. P. Fernandéz-Blázquez, J. P. Fuenzalida Werner, R. D. Costa, *Adv. Funct. Mater.* **2023**, *33*, 2300350.
[41] B. Lim, J. Kim, M. S. Desai, W. Wu, I. Chae, S.-W. Lee, *Biomacromolecules* **2023**, *24*, 118.
[42] X. Wang, Z. Li, W. Ying, D. Chen, P. Li, Z. Deng, X. Peng, *J. Mater. Chem. C* **2019**, *8*, 240.
[43] M. C. Gather, S. H. Yun, *Nat. Photonics* **2011**, *5*, 406.
[44] C. P. Dietrich, A. Steude, L. Tropf, M. Schubert, N. M. Kronenberg, K. Ostermann, S. Höfling, M. C. Gather, *Sci. Adv.* **2016**, *2*, e1600666.
[45] S. Chowdhury, M. Nieddu, M. Patrian, D. Gutiérrez-Armayor, L. M. Cavinato, J. P. Fuenzalida-Werner, M. G. Lleó, S. Ligi, R. D. Costa, *Adv. Mater. Technol.* 2301968.
[46] W. Li, Y. Pu, B. Ge, Y. Wang, D. Yu, S. Qin, *Int. J. Hydrog. Energy* **2019**, *44*, 1182.
[47] A. Mishra, M. K. R. Fischer, P. Bäuerle, *Angew. Chem., Int. Ed.* **2009**, *48*, 2474.
[48] V. Fernández-Luna, P. B. Coto, R. D. Costa, *Angew. Chem., Int. Ed.* **2018**, *57*, 8826.
[49] M. Chen, X. Fu, Z. Chen, J. Liu, W.-H. Zhong, *Adv. Funct. Mater.* **2021**, *31*, 2006744.
[50] M. Patrian, M. Nieddu, J. A. Banda-Vázquez, D. Gutierrez-Armayor, G. González-Gaitano, J. P. Fuenzalida-Werner, R. D. Costa, *Adv. Mater.* **2023**, *35*, 2303993.
[51] C. F. Aguino, M. Lang, V. Fernández-Luna, M. Pröschel, U. Sonnewald, P. B. Coto, R. D. Costa, *ACS Omega* **2018**, *3*, 15829.
[52] A. Espasa, M. Lang, C. F. Aguiño, D. Sanchez-deAlcazar, J. P. Fernández-Blázquez, U. Sonnewald, A. L. Cortajarena, P. B. Coto, R. D. Costa, *Nat. Commun.* **2020**, *11*, 879.
[53] A. Cao, Z. Ye, Z. Cai, E. Dong, X. Yang, G. Liu, X. Deng, Y. Wang, S. T. Yang, H. Wang, M. Wu, Y. Liu, *Angew. Chem., Int. Ed.* **2010**, *49*, 3022.
[54] Z. Cai, Z. Ye, X. Yang, Y. Chang, H. Wang, Y. Liu, A. Cao, *Nanoscale* **2011**, *3*, 1974.
[55] D. Gutiérrez-Armayor, Y. Atoini, D. Van Opdenbosch, C. Zollfrank, M. Nieddu, R. D. Costa, *Adv. Mater.* **2024**, *36*, 2311031.
[56] X. Wang, Y. Guo, Z. Li, W. Ying, D. Chen, Z. Deng, X. Peng, *RSC Adv.* **2019**, *9*, 9777.
[57] T.-T. Chen, J.-T. Yi, Y.-Y. Zhao, X. Chu, *J. Am. Chem. Soc.* **2018**, *140*, 9912.
[58] M. Hasler, M. Patrian, J. A. Banda-Vázquez, S. Ferrara, A. C. Stiel, J. Fuenzalida-Werner, R. D. Costa, *Adv. Funct. Mater.* **2024**, *34*, 2301820.
[59] R. Melikov, D. A. Press, B. Ganesh Kumar, S. Sadeghi, S. Nizamoglu, *J. Appl. Phys.* **2018**, *123*, 023103.
[60] P. B. Lawrence, J. L. Price, *Curr. Opin. Chem. Biol.* **2016**, *34*, 88.
[61] Q. Xiao, S. R. E. Draper, M. S. Smith, N. P. Brown, N. A. B. Pugmire, D. S. Ashton, A. J. Carter, E. E. K. Lawrence, J. L. Price, *ACS Chem. Biol.* **2019**, *14*, 1652.
[62] A. C. Fogarty, D. Laage, *J. Phys. Chem. B* **2014**, *118*, 7715.
[63] A. Zaghmi, A. A. Greschner, E. Mendez-Villuendas, J. Y. Liu, H. W. de Haan, M. A. Gauthier, *Data Brief* **2019**, *25*, 104037.
[64] U. Dahal, Z. Wang, E. E. Dormidontova, *Macromolecules* **2018**, *51*, 5950.
[65] M. I. Mohammed, F. El-Sayed, *Opt. Quantum Electron.* **2023**, *55*, 1141.
[66] E. Mousa, Y. Hafez, G. M. Nasr, *J. Electron. Mater.* **2021**, *50*, 2594.
[67] R. Nangia, N. K. Shukla, A. Sharma, *High Perform. Polym.* **2018**, *30*, 918.

[68] A. Ouahab, N. Cheraga, V. Onoja, Y. Shen, J. Tu, *Int. J. Pharm.* **2014**, *466*, 233.
[69] A. Abuchowski, T. van Es, N. C. Palczuk, F. F. Davis, *J. Biol. Chem.* **1977**, *252*, 3578.
[70] V. Fernández-Luna, D. Sánchez-de Alcázar, J. P. Fernández-Blázquez, A. L. Cortajarena, P. B. Coto, R. D. Costa, *Adv. Funct. Mater.* **2019**, *29*, 1904356.
[71] N. V. Visser, J. W. Borst, M. A. Hink, A. van Hoek, A. J. W. G. Visser, *Biophys. Chem.* **2005**, *116*, 207.
[72] K. M. Dean, J. L. Lubbeck, J. K. Binder, L. R. Schwall, R. Jimenez, A. E. Palmer, *Biophys. J.* **2011**, *101*, 961.
[73] A. Zaghmi, E. Mendez-Villuendas, A. A. Greschner, J. Y. Liu, H. W. de Haan, M. A. Gauthier, *Mater. Today Chem.* **2019**, *12*, 121.
[74] X. Shu, N. C. Shaner, C. A. Yarbrough, R. Y. Tsien, S. J. Remington, *Biochemistry* **2006**, *45*, 9639.
[75] F. V. Subach, V. V. Verkhusha, *Chem. Rev.* **2012**, *112*, 4308.
[76] H. L. Svilenov, T. Menzen, K. Richter, G. Winter, *Mol. Pharmaceutics* **2020**, *17*, 2638.
[77] J. L. Cleland, S. E. Builder, J. R. Swartz, M. Winkler, J. Y. Chang, D. I. C. Wang, *Nat. Biotechnol.* **1992**, *10*, 1013.
[78] J. L. Tubbs, J. A. Tainer, E. D. Getzoff, *Biochemistry* **2005**, *44*, 9833.
[79] F. V. Subach, G. H. Patterson, S. Manley, J. M. Gillette, J. Lippincott-Schwartz, V. V. Verkhusha, *Nat. Methods* **2009**, *6*, 153.
[80] O. V. Stepanenko, O. V. Stepanenko, D. M. Shcherbakova, I. M. Kuznetsova, K. K. Turoverov, V. V. Verkhusha, *BioTechniques* **2011**, *51*, 313.
[81] A. T. Pandelieva, M. J. Baran, G. F. Calderini, J. L. McCann, V. Tremblay, S. Sarvan, J. A. Davey, J.-F. Couture, R. A. Chica, *ACS Chem. Biol.* **2016**, *11*, 508.
[82] V. Krishnakumar, G. Shanmugam, *Ionics* **2012**, *18*, 403.
[83] B. Qiao, F. Jiménez-Ángeles, T. D. Nguyen, M. Olvera de la Cruz, *Proc. Natl. Acad. Sci* **2019**, *116*, 19274.
[84] W. W. Ward, in *Green Fluorescent Protein*, John Wiley & Sons, Ltd, New Jersey, USA **2005**, p. 39.
[85] L. Niklaus, H. Dakhil, M. Kostrzewa, P. B. Coto, U. Sonnewald, A. Wierschem, R. D. Costa, *Mater. Horiz.* **2016**, *3*, 340.